Transport in Porous Media (2019) 130:77–104
https://doi.org/10.1007/s11242-019-01289-9

Pore-Scale Simulations of Single- and Two-Phase Flow in Porous Media: Approaches and Applications

Thomas Ramstad[1] · Carl Fredrik Berg[2] · Karsten Thompson[3]

Received: 15 June 2018 / Accepted: 12 April 2019 / Published online: 22 May 2019

Abstract
We present a review of pore-scale simulations of immiscible fluid transport with focus on two of the most popular approaches: lattice Boltzmann modeling for direct simulations on digital models of the pore space and simulations on network models extracted from the pore space. This review focuses on covering basic theory and implementation strategies and gives the readers input and motivation to start their own pore-scale simulations and relate them to realistic porous media. We present a review of recent and relevant applications and how a digital workflow that combines advanced pore-scale imaging and simulations can give very useful input to different fields of science and industry, including reservoir characterization. Given the large span in methods and applications, this review does not aim to cover all methods or applications. However, it covers popular methods and describes to some extent their applicability to different types of transport problems.

Keywords Pore-scale modeling · Lattice Boltzmann methods · Pore-network simulation

1 Introduction

Simulation of transport in porous media can be divided into two categories separated by scale: The first is simulation of transport inside the individual pores constituting the pore space of the porous medium, e.g., solving the equations of motion inside the pore space where the pore walls are treated as no-flow boundaries. We will denote this first category as *pore-scale* simulations, and it will be the main focus of this article. The second category treats larger scales where it is possible to define averaged effective properties such as porosity

✉ Karsten Thompson
karsten@lsu.edu

Thomas Ramstad
trams@equinor.com

Carl Fredrik Berg
carl.f.berg@ntnu.no

[1] Equinor ASA, Arkitekt Ebbells veg 10, Rotvoll, Trondheim, Norway

[2] PoreLab, Department of Geoscience and Petroleum, Norwegian University of Science and Technology (NTNU), Trondheim, Norway

[3] Craft & Hawkins Department of Petroleum Engineering, Louisiana State University, Baton Rouge, USA

and permeability. However, these are *upscaled* properties from the smaller scales of porous media, and the physics and flow that take place on the pore scale ultimately determine how larger-scale flows must be treated.

For porous media in general, and in particular for reservoir rocks encountered in the extraction of hydrocarbons, the last decades have seen a huge rise in pore-scale simulations of transport. This rise has been facilitated by developments in computing power and pore-scale imaging. Simulations, in particular calculations directly on digital images of the pore space, are typically computationally heavy. It might seem counter-intuitive, but simulation on a model of physical size in the millimeter range could be orders of magnitude more computationally demanding than a model of physical size of kilometers.

This article focuses on the simulation side of digital pore-scale modeling. For such transport simulations to be predictive, they rely on representative models of porous media. There are two main approaches: direct flow simulation on pore-scale images and simulation on pore-network models. These two approaches are described in the two main sections of this review article.

We will concentrate on the lattice Boltzmann method (LBM) (Succi 2001) for simulation directly on grid or voxel representations of a porous medium. The LBM is a kinetic approach to hydrodynamics that is straightforward to implement on complex geometries, and it can incorporate small-scale physics while at the same time solve continuum fluid mechanics equations. These features make the LBM a popular and well-documented method for simulation of multiphase flow on the pore scale.

However, there exist several other methods that can be used for direct pore-scale flow simulations. Extensions to CFD methods like volume of fluid (VOF) (Raeini et al. 2012) and level-set (LS) (Sussman and Puckett 2000; Jettestuen et al. 2013) include fluid tracking functions that can incorporate local interfacial effects and at the same time solve continuum relations like Navier–Stokes equation. Lately, density functional methods like direct hydrodynamics (DHD) (Koroteev et al. 2014) have been applied to direct pore-scale simulations with promising results.

For pore-network modeling, several techniques will be discussed. The method of choice for obtaining a pore network is highly dependent on the material and the transport process to be modeled. As an example, electrical conductance depends on the total cross-sectional area of pores, whereas viscous fluid flow scales even more strongly, with an R_{eff}^4 functionality within individual pores, and therefore is more dependent on the largest pores and their interconnections.

Obtaining models of the porous medium, e.g., through micro-CT imaging, is its own field of research, and will be touched on only briefly in this article. However, we will discuss network extraction, which ties closely to the processing aspects of imaging workflows.

Porous structures are abundant on all length scales, and fluid transport in porous media has applications in almost all fields of material science and technology. Consequently, there is a huge body of literature on the subject, making it impossible to cover comprehensively in article form. This paper will therefore be colored by the authors selecting what we believe is most important for readers to be introduced to.

2 Lattice Boltzmann Method for Direct Pore-Scale Simulations

The lattice Boltzmann method (LBM) is a spatially discrete kinetic approach to hydrodynamics that solves a discretized Boltzmann equation of fluid particle distributions that move and collide on a regular lattice.

Many properties related to fluid–solid and fluid–fluid interactions can be implemented in a straightforward manner. Fluid–fluid interfaces can be automatically maintained, avoiding expensive interface tracking functions when treating multiphase flow. These features, combined with inherent parallelism and a programming simplicity for implementation on arbitrarily complex geometries, have made the LBM one of the most popular and well-documented methods for direct pore-scale flow simulations.

The theory and justification behind the LBM are thoroughly described in literature (Chen and Doolen 1998; Succi 2015) and text books (e.g., Rothman and Zaleski 2004; Succi 2001; Sukop and Thorne 2006; Guo and Shu 2013). In the following, we focus on the main features of the LBM and why they are well suited to address flow dynamics in complex geometries like porous media. Applications of flow modeling in porous media include single-phase flow (Succi et al. 1989; Jin et al. 2004), two-phase flow (Martys and Chen 1996; Chen and Doolen 1998), and digital rock physics (Ramstad et al. 2010, 2012).

2.1 The Lattice Boltzmann Equation

The LBM was originally developed empirically from the lattice gas automata (LGA) (McNamara and Zanetti 1988). Instead of the LGA Boolean fluid particles, the LBM handles fluid particle distributions, $f(x, v, t)$, which is the probability of one particle to be at position x with local velocity v at time t. This can be viewed as a pre-averaged version of the LGA using a Boltzmann equation formalism that leads to reduced intrinsic noise and improved collision rules.

The LBM corresponds to a spatial discretization of the Boltzmann equation, and the distribution f is restricted to the discrete nodes $\mathbf{x}$ on a regular lattice. To have a correct interpretation of the hydrodynamics, the lattice applied must exhibit the symmetry necessary to have mass and momentum conservation in addition to isotropy.

Commonly, the different lattice types are named $DnQm$ where n refers to the space dimension and m is the number of discrete velocity vectors $\mathbf{c}_i$. In Fig. 1, two of the most common mesh types are displayed: $D2Q9$ and $D3Q19$. They apply to two and three dimensions, respectively, and the lattices are composed of sub-lattices that contain velocity vectors of equal length. In addition, there is a rest distribution with a zero velocity vector $\mathbf{c}_o = 0$. A description of other lattice types can be found in, for example, Guo and Shu (2013).

The local density function is divided into parts $f_i(\mathbf{x}, t) = f(\mathbf{x}, \mathbf{v} = \mathbf{c}_i, t)$ that correspond to the directions of the discrete velocities $\mathbf{c}_i$.

Distribution dynamics can be summed up in the lattice Boltzmann equation (LBE), which combines advection and collision of the fluid distributions

$$f_i(\mathbf{x} + \mathbf{c}_i \Delta t, t + \Delta t) - f_i(\mathbf{x}, t) = \sum_j \Lambda_{ij}(f_j - f_j^{\mathrm{eq}}) + S_i(\mathbf{x}, t) \,. \tag{1}$$

The left-hand side of Eq. (1) is an advection term commonly referred to as *free streaming*. Fluid distributions can propagate to neighboring nodes with a rate proportional to, and in the direction of, discrete velocity vectors $\mathbf{c}_i$. This is in fact the only term that requires exchange of information with neighboring nodes. The rest of the terms are local.

The first term on the right hand side of Eq. 1 is a discrete *collision operator*, and the scattering matrix Λ_{ij} controls the relaxation of f toward a local pseudo-equilibrium distribution f^{eq}. In addition, a general source term $S_i(\mathbf{x}, t)$ can be applied that adds to the fluid distributions. Such terms are useful in applying additional physical effects like driving forces and local pressure fields. All terms on the right hand side of Eq. (1) are local in space and time.

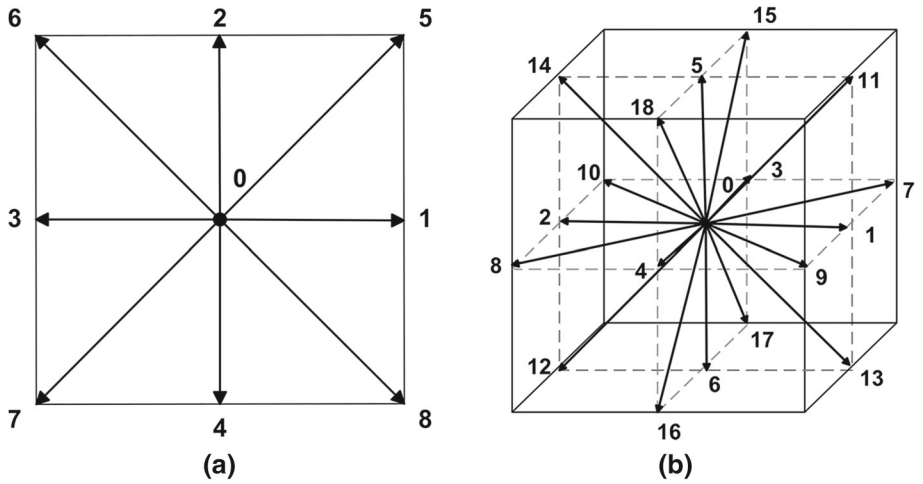

Fig. 1 Two of the most commonly used mesh types $D2Q9$ (**a**) and $D3Q19$ (**b**)

Hence, they can be computed without any need for broader communication on the lattice, which is an advantage for numerical implementation.

The pseudo-equilibrium function f^{eq} is a low-velocity Taylor expansion of the Maxwell–Boltzmann distribution function which is Gaussian in function form, yielding (Shan and He 1998):

$$f_i^{\text{eq}} = \rho w_i \left(1 + \frac{1}{c_s^2}\mathbf{c}_i \cdot \mathbf{u} + \frac{1}{2c_s^4}(\mathbf{c}_i \cdot \mathbf{u})^2 - \frac{1}{2c_s^2}|\mathbf{u}|^2\right) . \tag{2}$$

The discrete directions that correspond to the velocities c_i are given a set of weights w_i that normalize to unity. In addition, there is a defined speed of sound c_s that applies to the entire lattice.

The local mass and momentum at a node with position $\mathbf{x}$ at time t are given by the zeroth- and first-order kinetic moments of the fluid distributions

$$\rho(\mathbf{x}, t) = \sum_i f_i(\mathbf{x}, t) , \tag{3}$$

and

$$\rho\mathbf{u}(\mathbf{x}, t) = \sum_i f_i(\mathbf{x}, t)\mathbf{c}_i . \tag{4}$$

Higher-order kinetic moments than those in Eqs. (3) and (4) can be used to obtain other quantities like the local stress tensor from which the hydrostatic pressure can be derived. With an ideal-gas equation of state, the local pressure becomes $P = c_s^2\rho$ (Yuan and Schaefer 2006). However, other equations of state can be applied.

Mass–momentum transport is generally restricted to isothermal systems, since there is a fundamental lack of "thermal fluctuations" and energy dissipation in the LBM transport equations. Thermal flow implementations exist, but the native LBM is of a non-thermal nature (Li et al. 2016).

The truncation of the Maxwell distribution in Eq. (2) requires a limitation of low velocities, i.e., the Mach number is generally limited to $Ma = |\mathbf{u}|/c_s < 0.1$ (Succi 2015). Additionally, for Eq. (1) to reproduce the Navier–Stokes equation, it needs to be in the quasi-incompressible limit for small Knudsen numbers $Kn = \ell/L \ll 1$, meaning that the mean free path ℓ of

the fluid distributions is much shorter than the hydrodynamic length scale L. This can be interpreted as an expansion of the total particle distribution function into equilibrium and non-equilibrium parts $f = f^{\mathrm{eq}} + f^{\mathrm{neq}}$, and f^{neq} is only a small deviation from f^{eq} according to a Chapman–Enskog expansion (Chapman and Cowling 1970).

2.2 Relaxation Scheme

The local scattering matrix Λ_{ij} in Eq. (1) consists of constant coefficients and is difficult to handle directly. However, it is symmetric and can be reconstructed by a set of eigenvalues through a spectral decomposition.

A common approximation is to substitute the scattering matrix Λ_{ij} with only the leading, nonzero eigenvalue, $\lambda = -\omega$, and obtain the single-relaxation-time (SRT) lattice collision operator. This is also known as the Bhatnagar–Gross–Krook (BGK) collision operator (Bhatnagar et al. 1954). The relaxation parameter *omega* is the inverse of the relaxation time $\omega = 1/\tau$. Using the BGK operator, Eq. (1) simplifies to

$$f_i(\mathbf{x} + \mathbf{c}_i \Delta t, t + \Delta t) - f_i(\mathbf{x}, t) = -\omega(f_i(\mathbf{x}, t) - f_i^{\mathrm{eq}}(\mathbf{x}, t)) \,, \tag{5}$$

and is straightforward to implement (Guo and Shu 2013).

The relaxation parameter $\omega = 1/\tau$ is linked to the second-order kinetic moment of the fluid distributions, and thus, the kinematic viscosity of the fluid (with $\Delta t = 1$)

$$\nu = c_s^2 \left(\frac{1}{\omega} - \frac{1}{2} \right) . \tag{6}$$

From this relation, it is clear that the relaxation parameter needs to be in the region $0 < \omega < 2$ to give positive viscosity.

The simplicity of the BGK method has made it a popular implementation for the LBM, but it has some limitations in the formalism. The implicit relationship between the single relaxation parameter and the fluid viscosity can lead to numerical instabilities for low viscosities. With only one relaxation parameter, the relaxation time will be the same for all higher-order kinetic moments. Such a simplification may cause problems for certain fluid systems with relaxation processes on different time scales (Premnath and Abraham 2007).

One way to address some of the notable shortcomings associated with the lack of tuning parameters in the BGK implementation is by introducing multiple relaxation times (MRT) (d'Humières 2002). The MRT method introduces additional relaxation parameters for higher-order kinetic moments based on the scattering matrix of Eq. (1). However, the scattering matrix Λ needs to be eigen-decomposed in order to be used in such a formalism. This can be done with an invertible transformation matrix $\mathbf{M}$. The updated collision operator reads

$$\sum_j \Lambda_{ij}(f_j - f_j^{\mathrm{eq}}) = -\mathbf{M}^{-1} \hat{\Lambda} \mathbf{M}(f - f^{\mathrm{eq}}) \,, \tag{7}$$

where $\hat{\Lambda} = \mathrm{diag}(\omega_0, \omega_1, \omega_2, \ldots, \omega_q)$ is the diagonal collision matrix that now includes q individual relaxation parameters.

In practice, the collision is done by first transforming the particle distributions into moment distributions $m = \mathbf{M} f$ in order to operate in the momentum space with a set of pseudo-equilibrium distributions m^{eq} and then transfer back to the position space before streaming is performed similarly to the BGK implementation.

A scheme with two relaxation parameters (TRT) has been introduced where the collision can still be done in the position space (Ginzburg et al. 2008). With this type of hybrid

collision scheme, costly transformation to and from the momentum space can be avoided. Other collision schemes in position space that enhance stability (Latt and Chopard 2006) and use multiple relaxation parameters (Shan and Chen 2007) have been introduced in recent years.

2.3 Implementation on the Pore Space

In this section, we will describe in more detail the practical use of LBM for simulating flow in porous media directly on digital images. The geometries where transport takes place are usually heterogeneous and complex. Additionally, we want to move from one to two fluid phases. The methods, therefore, must include treatment of fluid/solid and fluid/fluid interactions.

2.3.1 Wall Boundary Conditions

Solid–fluid interaction is a central part of how to model flow in complex boundary geometries. First of all, a regular LBM lattice that incorporates the symmetries discussed in the previous section has to be applied to a digital model of a porous medium. This results in many nodes in the lattice becoming solid particles rather than density populations, and such solid nodes affect collisions.

The most common type of wall treatment for LBM in porous media is the no-slip boundary condition. This boundary condition halts the near-wall particle distribution and prohibits particles from propagating parallel to the wall. Effectively this can be done by, for example, a halfway bounce-back, where a fluid distribution that propagates onto a solid node is reflected after the collision step back into the fluid domain as

$$f_{\bar{i}}(\mathbf{x}_f, t + \Delta t) = f_i^*(\mathbf{x}_f, t) \, . \tag{8}$$

Here $\mathbf{x}_f$ represents a fluid node bordering to a solid, and f_i^* is the local post-collision distribution with $c_i = -c_{\bar{i}}$ (see Fig. 2).

The simple treatment of wall boundaries makes it rather straightforward to apply the LBM directly on complex geometries such as the microstructure of porous media. However, there are issues related to accuracy, as the resolution has to be high enough to ensure the adequate treatment of the local physics and conservation rules. The halfway bounce-back scheme obtains second-order accuracy only if the wall is positioned precisely halfway between a solid and fluid node (as compared to second-order accurate for bulk collisions). A staircase implementation for real geometries as illustrated in Fig. 2 may limit the halfway bounce-back scheme to lower order accuracy (Ginzbourg and Adler 1994).

To increase accuracy of the bounce-back wall treatment, different interpolation schemes have been introduced (Pan et al. 2006). However, they mostly come with the cost of increased complexity and reduced numerical stability.

For no-slip shear flows, the effective wall placement can be dependent on the relaxation scheme parameters (Manwart et al. 2002). For the BGK relaxation scheme with only one relaxation parameter, there is a viscosity-dependent slip velocity which affect the overall velocity field. Consequently, it will lead to a viscosity dependency in calculation of, for example, permeability. This is a major shortcoming of the BGK method, but the problem can be reduced by introducing more relaxation parameters in a multiple relaxation time scheme (MRT).

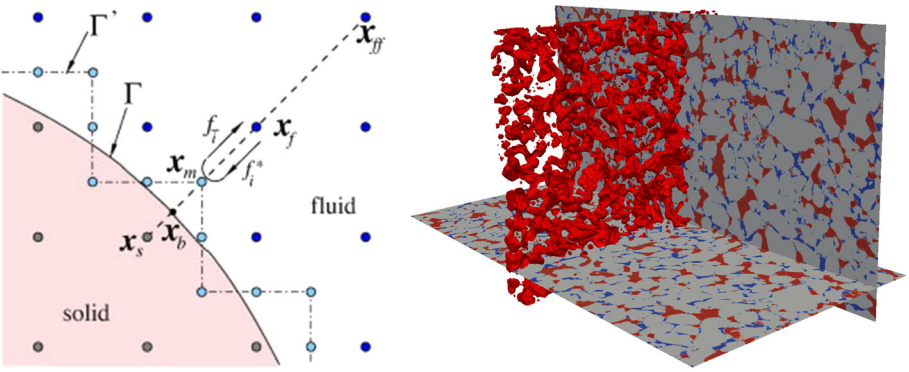

Fig. 2 The left graphic illustrates the halfway bounce-back scheme implemented on a smooth boundary surface Γ. The wall is interpreted as halfway between the solid x_s and fluid nodes x_f, i.e., $x_b \rightarrow x_m$ giving rise to a staircase wall boundary Γ'. The graphic is taken from from Yin and Zhang (2012). The right image shows a snapshot of in situ fluid distribution after a two-phase LBM simulation on a digital image of a sandpack. The 3D illustration of oil fluid clusters (red) shows complex interface geometries, while the 2D projection to the pore space exhibits local wetting effects in the solid–fluid interfaces

There have also been many attempts to resolve lack of resolution in LBM grids from digital images, e.g., with adaptive grid refining (Tölke et al. 2006). Sub-resolution microporosity can be treated with a partial bounce-back scheme (Grey LBM) (Zhu and Ma 2013). However, while such techniques may work well in some cases, they can also introduce too much complexity, especially when handling multiphase flow.

2.3.2 Driving the Flow

The simplest way to apply a driving force to the fluid distribution, is by adding a momentum source term to each density distribution in the LBE Eq. (1). With a uniform body force $\mathbf{F}$ acting on the system, the source term can be written as $S_i(\mathbf{x}, t) = w_i \rho \mathbf{F} \cdot \mathbf{c}_i$.

A uniform body force F_x over the entire lattice in the flow direction x will alter the global momentum balance. The local pressure is changed to $P' = P - F_x x$, making it equivalent to introducing a pressure gradient. There exist other implementations of body-force schemes (Buick and Greated 2000; Guo et al. 2002), but they all affect the local momentum of the fluids.

Periodic external boundaries at the inlet and outlet of a system combined with a body force will reduce finite size effects (Ramstad et al. 2010). This is convenient when handling real porous media in, for example, permeability calculations (Jin et al. 2004).

The other obvious approach is open boundaries with a constant pressure or velocity profile on the inlet adjusted by the inlet fluid distributions (Zou and He 1997; Hecht and Harting 2010)

$$f_{\text{inlet}}(\mathbf{x}, t) = f^{\text{eq}}_{\text{inlet}}[\rho_{\text{in}}, u(\mathbf{x})_{\text{in}}] \,. \tag{9}$$

Particle distributions that leave the model at each end will disappear from the system.

Open boundary conditions allow for better control of inlet flow, but also introduce larger finite size effects. These are especially apparent on the outlet, where discontinuities in the flow profile may arise (Succi 2001).

2.3.3 Physical Units

For the LBM, the fluid dynamics are constrained to a lattice. In order to compare the results to a physical system, the lattice quantities need to be converted from lattice to physical units. This procedure requires a set of fundamental scaling units that are characteristic for the physical system, i.e., physical length l_p, fluid density ρ_p and time t_p. The length l_p is usually defined as the lattice constant, i.e., the distance between the nodes, and the density ρ_p is determined by the fluid. The time scale t_p must be set to give consistency with other physical quantities such as pressure $P_{\text{phys}} = P_{\text{lattice}}(\rho_p l_p^2/t_p^2)$ and viscosity $\nu_{\text{phys}} = \nu_{\text{lattice}}(l_p^2/t_p)$ (Ramstad et al. 2012).

2.4 Immiscible Multiphase Flow

The natural separation of immiscible fluids gives rise to surface tension and local capillary forces. Understanding these local capillary effects is essential when defining constitutive relations with upscaled parameters such as relative permeability and capillary pressure.

There exist several methods for treating immiscible fluids in the LBM. The most widely used for applications to porous media is the color gradient method (Gunstensen et al. 1991; Latva-Kokko and Rothman 2005a) and pseudo-inter-particle potential (Shan and Chen 1993) with modifications (Martys and Chen 1996; Huang et al. 2007). However, other methods exist as well, e.g., the free energy (Swift et al. 1995; Yang and Boek 2013) and mean-field methods (He et al. 1999).

Generally, the fluid phases need to be treated separately

$$f_i(\mathbf{x}, t) = \sum_{\alpha} f_i^{\alpha}(\mathbf{x}, t) \ , \tag{10}$$

where α denotes the fluid phase. All methods basically introduce interfacial tension (IFT), which balances the pressure difference between the phases α by adding an extra perturbation force term to the source term in Eq. (1). The main differences arise in how the phase separation is treated.

One of the largest issues for LBM multiphase flow relates to non-physical currents near fluid–fluid and fluid–solid interfaces. These are commonly referred to as spurious or parasite currents (Connington and Lee 2012; Shan 2006). Because of the limited degrees of freedom in the LBM collision scheme, there is no easy way to fix the problem. However, certain phase-separation schemes can reduce the problem (e.g., the free energy and entropic method Yang and Boek 2013; Mazloomi et al. 2015).

In this paper, we only mention what we consider to be the two most frequently applied methods for immiscible two-phase flow in porous media. A recent review by Liu et al. (2016) treats several other phase-separation methods for LBM in detail.

2.4.1 Color Gradient Method

Color gradient phase separation (CG) was first introduced by Gunstensen et al. (1991), with several modifications since (e.g., Grunau et al. 1993; Latva-Kokko and Rothman 2005a).

For most two-phase applications, the total fluid distribution function in Eq. (10) is split into a binary fluid system containing a "Red" and "Blue" fluid phase $f_i = f_i^R + f_i^B$. The CG method for two-phase flow will calculate a perturbation to the collision operator based on the gradient between the fluid phases

$$\mathbf{g} = \sum_i [\rho_R(\mathbf{x} + \mathbf{c}_i) - \rho_B(\mathbf{x} + \mathbf{c}_i)]\mathbf{c}_i \ . \tag{11}$$

The source term in Eq. (1) is then reformulated as:

$$S_i' = S_i + A|\mathbf{g}| \left(w_i \frac{(\mathbf{c}_i \cdot \mathbf{g})^2}{|\mathbf{g}|^2} - B_i \right) , \tag{12}$$

where A is a tunable parameter that is directly proportional to the IFT strength σ. Parameters B_i are predefined weights for the different directions. Commonly, the weight parameters are fixed, e.g., $B_i = \frac{1}{2}$ for all i, but a differentiation of B_i in the different directions will better preserve mass and momentum locally and reproduce correct continuum equations (Reis and Phillips 2007).

Phase separation is maintained by maximizing the color gradient through a recoloring operator. To reduce pinning of surfaces, Latva-Kokko and Rothman (2005a) introduced the following

$$\begin{aligned} f_i^R &= \frac{\rho_R}{\rho} f_i^* + \beta \frac{\rho_R \rho_B}{\rho^2} \cos\phi \, f_i^{\text{eq}} \, |_{\mathbf{u}=0} \ , \\ f_i^B &= \frac{\rho_B}{\rho} f_i^* - \beta \frac{\rho_R \rho_B}{\rho^2} \cos\phi \, f_i^{\text{eq}} \, |_{\mathbf{u}=0} \ , \end{aligned} \tag{13}$$

where f_i^* is the distribution after the LBE collision of Eq. (1) when applying the updated source term in Eq. (12). β controls the width of the fluid interface, and ϕ is the angle between the color gradient $\mathbf{g}$ and the lattice velocity $\mathbf{c}_i$.

The CG algorithm has some favorable features when it comes to applications of two-phase immiscible flow in porous media. Phase separation with a relatively sharp interface is ensured, and the parameter A can be scaled linearly from the surface tension σ. However, lack of resolution and a large absolute value of the color gradient may lead to numerical instabilities. There are also limitations to the viscosity and density ratio between the fluids (Liu et al. 2016).

2.4.2 Inter-particle Potential Method

The other main phase-separation method is the inter-particle potential method, most notably the Shan–Chen (SC) method (Shan and Chen 1993). Phase separation is treated through pseudo-potentials, $G_{\alpha\tilde{\alpha}}(\mathbf{x}, \mathbf{x}')\psi_\alpha(\mathbf{x})\psi_{\tilde{\alpha}}(\mathbf{x}')$, where the potential strength can be tuned with the Green's function, $G_{\alpha\tilde{\alpha}}(\mathbf{x}, \mathbf{x}')$.

The collision of the fluids is treated separately, while a separating force is added to the collision operator depending on the potential ψ for fluid phases α and $\tilde{\alpha}$

$$\mathbf{F}_\alpha = -G\psi_\alpha(\mathbf{x}, t) \sum_i w_i \psi_{\tilde{\alpha}}(\mathbf{x} + \mathbf{c}_i, t)\mathbf{c}_i \quad \text{for} \quad \alpha \neq \tilde{\alpha} \ , \tag{14}$$

where the potential strength is set to $G_{\alpha\tilde{\alpha}} = G$, for a two-phase fluid system. There exist several forms of the potential, but the simplest is $\psi_\alpha = \rho_\alpha$. The separation of the phases takes place at a critical strength G_c. This approach can accommodate near-miscible transitions, which is not possible with the CG method. On the other hand, the interface is more diffuse, which is problematic for low-resolution grids (relative to pore geometry). In addition, the surface tension σ has a nonlinear relation to the potentials, which complicates the setup of the model.

The original Shan–Chen implementation used a local velocity shift force scheme, where the velocity $\mathbf{u}^{\text{eq}}$ of the pseudo-equilibrium distribution of the specific phase f_α^{eq} will change according to the force in Eq. (14):

$$\mathbf{u}_\alpha^{\text{eq}} = \mathbf{u} + \frac{\tau}{\rho}\mathbf{F}_\alpha \ . \tag{15}$$

The local potentials will change the equation of state, and the local pressure takes the form, $P = c_s^2\rho + \frac{c_s^2}{2}\sum_{\alpha,\tilde{\alpha}} G_{\alpha\tilde{\alpha}}\psi_\alpha\psi_{\tilde{\alpha}}$.

2.4.3 Wettability

Wettability describes the relative affinity of the fluids to the solid and is one of the most influential properties affecting how immiscible fluids behave in a porous medium (Anderson 1987). As can be seen from Fig. 2, the in situ fluid distribution will depend heavily on how the wettability is implemented in LBM.

On a plane surface, this relative affinity is measured by a contact angle θ that quantifies the surface tension balance between the solid and the two fluid phases with mutual interfacial tension σ:

$$\cos\theta = \frac{\sigma_{nw} - \sigma_w}{\sigma} \ , \tag{16}$$

where nw and w denote non-wetting and wetting fluids.

The various LBM phase-separation methods treat wettability through fluid–solid interaction, and the resulting affinity of a fluid phase to the solid surface. In the CG algorithm, the contact angle is controlled by a parameter η that controls the phase gradient at the solid nodes, i.e., the red-wall gradient element is $|\mathbf{g}_{\text{red-wall}}| = |f^R - f_{\text{red-wall}}| = \rho(1-\eta)$ (Latva-Kokko and Rothman 2005b). With similar definition for the blue phase, these gradient elements are added to the total gradient in Eq. (11). Combined with Eq. (16), the expression for the contact angle in the CG method becomes

$$2\rho\cos\theta = \rho(1+\eta) - \rho(1-\eta) \ , \tag{17}$$

and hence $\cos\theta = \eta$. This simple approach to fluid–solid interactions gives the correct affinity of one fluid to a plane wall, but it is argued that it introduces errors for more complex geometries. A more thorough treatment of the orientation of the wall-fluid color gradient has been proposed recently (Leclaire et al. 2017; Akai et al. 2018).

For the Shan–Chen method, the wettability is interpreted as an adhesion potential G_a for the phases to the wall. Hence, a fluid–solid force term similar to the fluid–fluid force in Eq. (14) is defined as

$$\mathbf{F}_\alpha^{f-s} = -G_{a,\alpha}\psi_\alpha(\mathbf{x},t)\sum_i w_i s(\mathbf{x}+\mathbf{c}_i,t)\mathbf{c}_i \ , \tag{18}$$

where $s \in [0,1]$ refers to a fluid or solid node.

3 Pore-Network Modeling

Direct modeling of multiphase flow on digital images of the pore space may seem like the most natural choice for pore-scale modeling. However, this approach often generates large models that are computationally demanding, sometimes unfeasible to run even on modern

high-performance computers. Additionally, many of the pore-scale flow processes require high resolution, which adds to the computational difficulties.

A common way to reduce the size of the computational model (for an equivalent-size physical domain) is to replace the digital image of the pore structure by representative pore elements connected as a network, commonly referred to as pore-network modeling (PNM). The elements in a pore network are usually identified as pore bodies that are connected through pore throats. The geometrical shape of the bodies and throats in the pore network are idealized, but should represent volumes and shapes in the actual porous medium to a reasonable degree. Additionally, modern networks retain the topology, pore locations, spatial correlations, and pore volumes of the porous medium from which they were mapped.

The extraction of a network analogue of the pore space can be a challenging process. Most of the geometrical structure of the individual pores is sacrificed in the transformation from image voxels to the network elements consisting of individual pore bodies and throats. The trade-off for this compromised description of the pore space is that a network model operates with analytic or semi-analytic models applied to the network elements, which in turn allows for "infinite-resolution" modeling of features such as wetting films along with dramatic improvements to computational efficiency in most cases, compared to direct methods.

Due to scope and size limitations, this section will invariably give a limited introduction to network modeling. Other review papers have a more in-depth coverage of the pore-space characterization (Bultreys et al. 2016), network construction (Bultreys et al. 2016; Xiong et al. 2016), dynamic algorithms (Joekar-Niasar and Hassanizadeh 2012) and applications (Blunt et al. 2013). For a more unabridged treatment, please refer to the recent book by Martin Blunt which gives a comprehensive treatment of the subject (Blunt 2017).

3.1 Background

Network modeling of flow in porous media started with the seminal work of Fatt (1956). Throughout the years, and fueled by increasing computational power, pore-network models became an increasingly popular tool for investigating fundamental flow processes and patterns in porous media. This effort was in many cases combined with growth modeling and invasion percolation theory.

Early pore-network models were derived from experimental micro-model analogues (e.g., etched glass models), where the shape and structure of the pore bodies and connecting throats are relatively simple (Lenormand et al. 1984). Direct extraction of pore networks from such porous media was rarely applied. Instead, networks were constructed in a stochastic manner from a given distribution of geometrical shapes such as capillary tubes, mapped onto a regular lattice topology.

More effort was put into the description and handling of the fluid propagation and displacement through the pore network. This was modeled both dynamically, with time-dependent fluid propagation (Koplik and Lasseter 1985), and with a quasi-static approach in which any fluid displacement is controlled by capillary forces (Øren et al. 1998). Either way, such simulation results have been extensively compared to experimentally observed flow patterns and measured quantities. The combination of pore-network simulation and micro-model experiments has given increased insight into phenomena such as viscous and capillary fingering, drainage and imbibition processes, and trapping mechanisms.

In two-dimensional networks where occupancy of network elements is restricted to only a single phase, then only one phase can be continuous throughout the model. To remedy this

shortcoming, network models were extended to three dimensions in Chatzis et al. (1977). However, the authors concluded that this was not enough to obtain realistic models.

As only one phase is continuous through the model, two-phase flow in water-wet micro-models exhibits significant ganglion dynamics. Such dynamics of displacement of disconnected oil ganglias was investigated by two-dimensional square lattice network models by Payatakes (1982). Following this work, several other authors also simulated multiphase flow in square lattice network models (Lenormand et al. 1984; Chen and Koplik 1985). Simulation results were comparable to experimental micro-model flooding results for primary drainage and had qualitative similarities for imbibition processes. Dynamic network models were later extended to three-dimensional networks (Blunt and King 1991).

A pertinent question that quickly arose was whether pore-network models could be used to predict flow properties such as capillary pressure and relative permeability from specific samples of porous rocks and core material. To address this issue, the pore networks would have to be extracted from naturally occurring porous structures, and the fluid displacement handled in a realistic way (including fluid properties and wettability).

Advances toward realistic geometries for network models came when networks were extracted from sphere packs (Roberts and Schwartz 1985; Bryant and Blunt 1992; Bryant et al. 1993), in contrast to earlier networks being regular lattices. A further advance toward realistic networks came with the digital reconstruction of a Bentheimer sandstone by simulating the rock forming processes of sedimentation, compaction and diagenesis (Bakke and Øren 1997). A pore network was extracted from the simulated sandstone model, and multiphase flow was simulated on the extracted network. The network simulation allowed more than one fluid to simultaneously occupy pore throats, and the resulting relative permeability curves gave a remarkably good match with experimental data.

3.2 Network Model Extraction

Extraction of a model for the pore space of the porous medium is an essential first step for pore-network modeling. The network consists of nodes and links, where the nodes represent pore bodies and the links represent the pore throats connecting the pore bodies. A porous medium and its extracted network are shown in Fig. 3, where a traditional ball-and-stick representation is used to visualize the network. A pore body is understood as a larger cavity in the porous medium, while a pore throat is a local constriction connecting two pore bodies. There is, however, no exact definition of a pore body or a pore throat. Consequently, there is no unique way to define the pore network of a porous medium. In general, for the network model to be a representative simplification of the pore space, it should preserve the topology of the pore space. Additionally the network elements need associated geometrical information, e.g., volume, length, cross-sectional area, etc., enabling the calculation of transport properties such as hydraulic and electric conductances.

As mentioned above, network models became more realistic when they were based on sphere packs (Roberts and Schwartz 1985; Bryant et al. 1993). For sphere packs, the network extraction was based on a Voronoi partitioning of the space using the sphere centers as seeds for the partitioning (Mason 1971). The nodes in the network, representing pore bodies, were points equidistant from the four nearest sphere centers. The links, representing pore throats connecting the pore bodies, were defined by points equidistant from three of the spheres associated to a node. This way, all the nodes were connected by exactly four links, yielding a uniform topology where the coordination number was exactly four (except at boundaries). The hydraulic and electrical conductances assigned to the links were estimated based on the

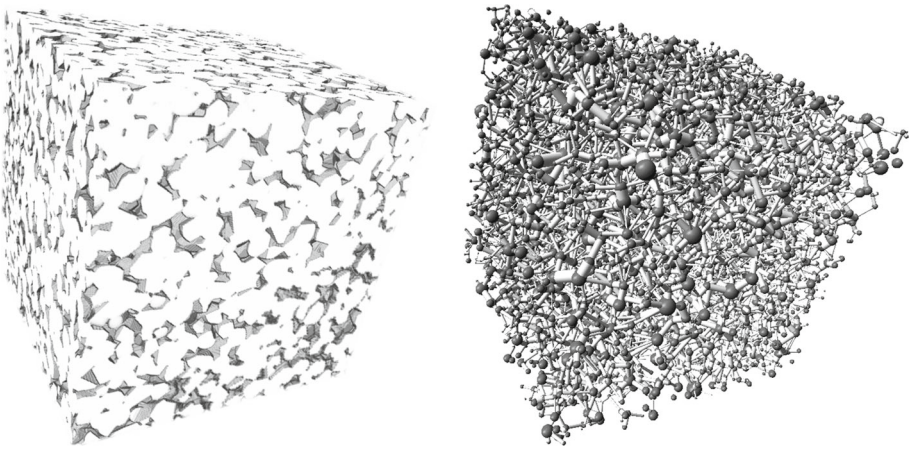

Fig. 3 Three-dimensional visualization of a Fontainebleau rock model from Berg and Held (2016), and its corresponding pore network from Berg (2014). The network has been extracted using a grain-based method similar to the method described in Bakke and Øren (1997)

pore structure in the cross section defined by the Voronoi edge given by the three spheres defining the link. Such network models were able to predict the electrical conductivity of fused glass beads (Roberts and Schwartz 1985) and the permeability of sphere packs (Bryant et al. 1993).

More complex structures, e.g., captured from micro-CT images of natural porous media, do not have the simpler structure of a sphere pack and therefore require other methods for network extraction. The essential topology of the pore space can be obtained from the medial axis; the set of points equidistant from two or more points at the matrix-void surface (Lindquist et al. 1996). The medial axis is sensitive to surface irregularities and yields a high number of dead ends. To remedy such unwanted features, a skeleton of the pore space can be obtained by the centers of maximal spheres: Let $\mathcal{B}$ be the set of all spheres inside the pore space. Then, $\mathcal{M} = \{S \in \mathcal{B} \mid S \not\subset T \, \forall T \in \mathcal{B}\}$ is the set of maximal spheres, and the skeleton $\mathcal{S}$ is the centers of the maximal spheres $\mathcal{M}$ (Thovert et al. 1993). The backbone of the skeleton $\mathcal{S}$ preservers the topology of the pore space without including dead ends arising from corners and irregular surfaces. Voxels in the backbone of $\mathcal{S}$ containing more than two neighbors can be considered as nodes in the pore network, while voxels having exactly two neighbors are part of the links connecting the nodes (Liang et al. 2000). This methodology yields networks consisting almost entirely of nodes with coordination number three. Algorithms to improve the network by merging nodes must avoid several pitfalls, e.g., creating links where both ends are connected to the same pore (Sheppard et al. 2005).

When digital reconstruction of a porous medium starts with grain sedimentation, the grain centers can be used as a basis for the network extraction (Bakke and Øren 1997). The grains can then be fully dilated, and the backbone of the pore network is given by the contact of two or more surfaces between the dilated grains. Network extraction incorporating information about the individual grains tends to be more stable. An example of a network extracted using a grain-based method is visualized in Fig. 3. Without information on the location of the individual grains, e.g., in a micro-CT image of the pore space, a grain-based network extraction can still be employed after a grain identification algorithm has been applied to the matrix (Thompson et al. 2006). For some structures, grain segmentation can yield a high number of artifacts, thereby inhibiting grain-based network extraction.

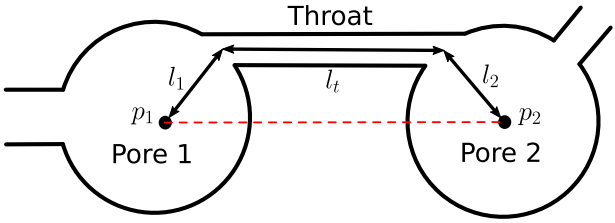

Fig. 4 A visualization of the different element in the calculation of the hydraulic conductivity of a link in the network model

3.3 Single-Phase Flow

For realistic simulation of slow single-phase flow, the network representation of the porous medium must properly capture the underlying topology and geometry of the pore space (Koplik 1982). Each node and link has a spatial description given by a point $x \in V$. Nodes and/or links also have associated volumes, and the volume of all pore elements should sum to the total pore volume.

Multiple methods are used to distribute volumes and resistances onto a network. Two of the most common ways are (1) to assign volume to the pores and resistance to throats, or (2) to divide volume and/or resistance between pores and connecting throats based on local geometry. While quite different conceptually, the differences get sorted out in the specific network modeling equations used in each case, making the choice largely a matter of preference.

We will focus on the latter approach to keep the discussion consistent. As such, we define the distance between pore body 1 and pore body 2 connected by a pore throat t as divided into parts: l_1 and l_2 are associated with each pore body, and l_t is associated with the pore throat, as seen in Fig. 4. With such a division of the pore space, it is common to assume a single pressure value associated with the nodes, and thus a pressure gradient along the links. Such a division will in effect yield the nodes as volume-free junctions for the connecting links. One would then need to divide the pore body volume among the connecting links.

To describe the hydraulic (or electrical) conductance for the links, it is common to introduce a shape factor $G = A/P^2$, where A is the cross-sectional area and P is the perimeter of the pore under consideration (Mason and Morrow 1991). The hydraulic conductance of each network element can then be approximated by

$$g = \frac{3r^4}{80\mu G}, \tag{19}$$

where r is the inscribed radius of the pore (Øren et al. 1998).

The effective hydraulic conductance between two pore bodies 1 and 2 connected by a pore throat t is taken as the length-weighted harmonic average of the three elements as

$$g_{1,2} = l_{1,2}\left(\frac{l_1}{g_1} + \frac{l_t}{g_t} + \frac{l_2}{g_2}\right)^{-1}, \tag{20}$$

where $l_{1,2} = l_1 + l_t + l_2$, see Fig. 4. Assuming a Hagen–Poiseuille-type relation between the fluid discharge $Q_{1,2}$ from pore 1 to pore 2 and the pressure gradient $\nabla p_{1,2} = (p_2 - p_1)/l_{1,2}$ for each pore throat t, we have

$$Q_{1,2} = -g_{1,2}\frac{p_2 - p_1}{l_{1,2}}, \tag{21}$$

where p_i is the pressure associated with pore body i.

The above description allows for the calculation of an absolute permeability (or similarly, the electrical conductance). Due to mass balance, we must have the following equation for each node i:

$$\sum_j Q_{i,j} = 0, \tag{22}$$

where the summation runs over all links j connected to node i. Solving for the pressures in each node requires inversion of a sparse matrix of dimension equal to the number of nodes. The resulting pressure drop and volumetric flow rate for the whole network yield the predicted absolute permeability. Comparing the network permeability with the permeability obtained from grid-based simulations on the same pore structure is one verification that the network model is representative of the pore structure.

Other types of transport, e.g., electrical current or steady-state diffusion, can easily be implemented with the same type of network models by updating the network conductances for the relevant transport process and applying an appropriate conservation equation.

3.4 Multiphase Flow

The attributes that make pore-network modeling appealing in general are particularly important for modeling immiscible displacement and multiphase flow. These processes are nonlinear and usually transient, meaning computational efficiency is essential. Additionally, multiphase flow is influenced by wetting films (thin and thick) that can be difficult to resolve using a grid-based simulation, and by fast non-equilibrium events that are impractical to resolve with time stepping. Hence, the prospect of simulations that can avoid these numerical limitations is highly desirable. Of course, the complexities of multiphase flow can also serve to magnify the approximations and limitations inherent in pore-network approximations if modeling is not done carefully.

Although other types of multiphase flow can be modeled using pore networks, we restrict the discussion in this section to two-phase flow due to space limitations and because it provides the foundation for more specialized modeling.

3.4.1 Quasi-static Algorithms

Fatt's original work on network modeling (Fatt 1956) addressed capillary pressure behavior and used a version of algorithms that are still common today for simulating zero-capillary-number displacements. They are termed quasi-static, which refers to the fact that the numerical displacement is performed by tracking a series of pore or throat invasions that are based on static (equilibrium) interface configurations within the pore space, as the applied capillary pressure is increased or decreased. Accurate quasi-static algorithms remain important because they simulate porosimetry, so are used to numerically generate capillary pressure curves from digital images.

In its simplest form, quasi-static drainage is equivalent to bond invasion percolation, while quasi-static imbibition is equivalent to site percolation. In practice, this can be complicated by a number of factors, a few of which are summarized here.

Although the quasi-static restriction keeps the rule-based numerics simple, these rules do require predicting limiting capillary pressures for local invasions or retractions at each

step in the displacement process. Strictly speaking, this means knowledge of equilibrium interface configurations as a function of capillary pressure anywhere in the pore space, which is a daunting task for any real porous medium. This challenge highlights an advantage of the network approach for this application: transformation of the pore space into geometric elements gives us a better chance of solving for local interface geometries.

The Young–Laplace equation links the capillary pressure P_c over an interface to the interfacial tension σ and the principal radii of curvature r_1 and r_2 as

$$P_c = \sigma \left(\frac{1}{r_1} + \frac{1}{r_2} \right). \tag{23}$$

For a cylindrical pore of radius r where the interface has a contact angle θ with the pore wall, the principal radii are $r_1 = r_2 = r/\cos\theta$, thus

$$P_c = \frac{2\sigma \cos\theta}{r}. \tag{24}$$

The problem with spherical/cylindrical pores and tubes is that they cannot accommodate the thick wetting films and corner flows that affect multiphase flow. For this reason, pore networks often use shapes such as triangles for the cross section, which give more realistic but still tractable relations between the capillary pressure and the pore size based on minimization of free energy (Mayer and Stowe 1965; Princen 1969a, b, 1970; Mason and Morrow 1991). Assuming a triangular pore throat of constant cross-sectional area, then the drained wetting fluid remaining in a corner would have one principal axis of infinite radius, while the other will have a radius r. Thus, the Young–Laplace equation gives:

$$P_c = \frac{\sigma}{r}. \tag{25}$$

This relationship allows the model to capture the reduction in wetting fluid in the corners as the capillary pressure increases during the drainage process, for instance.

Once a network geometry has been defined that allows capillary pressure estimates to be made, a quasi-static primary drainage process can be simulated (Chandler et al. 1982). The process begins with the network fully saturated with wetting fluid, and one network element at a time is filled with the invading non-wetting fluid. At each step, the drainage continues through the pore throat with the lowest associated capillary pressure that is connected to a pore body filled with non-wetting phase or connected to the inlet (Wilkinson and Willemsen 1983). The simulation mimics mercury intrusion measurements used to generate capillary pressure curves (Yuan and Swanson 1989).

During subsequent imbibition of a wetting phase displacing the non-wetting phase, two main mechanisms occur. The first is movement of the terminal menisci leading to direct filling of pores and throats from adjacent pores already filled with the wetting phase. The second is swelling of the wetting layers as indicated by Eq. (25), yielding movement of the arc menisci and possible snap-off of the non-wetting phase (Lenormand et al. 1983, 1984).

Simulating quasi-static movement of the terminal menisci through pore throats is a similar process to primary drainage discussed above, using relations between capillary pressure and pore geometry. However, there can be hysteresis in the contact angle, yielding different threshold pressures than in the drainage case. Additionally, the algorithm must account for cooperative filling, meaning the threshold capillary pressure for filling a pore body is strongly affected by the number of adjacent pore throats already filled by the wetting fluid. Numerical algorithms for cooperative filling have followed the famous experiments and theory from Lenormand et al. (1983), which are relevant for a 2D geometry with pore coordination

number of four. While the same physics apply to more realistic 3D geometries, a generalized approach for modeling cooperative filling (within the simplified structure of pore-network modeling) has proved elusive. Hence, most imbibition algorithms rely on simple coordination number rules that make the critical capillary pressure a function of the number of adjacent pore throats filled with wetting phase (but not the actual interface geometry that could be created by cooperative filling in that pore) (Lenormand et al. 1988; Blunt and Scher 1995).

The second important displacement process during imbibition is snap-off. Wetting layers swell as the capillary pressure is reduced, and at some point the non-wetting phase loses contact with the surface creating an unstable interface and the wetting phase will spontaneously fill the throat. Like cooperative filling, snap-off criteria depend on the specific local geometry of the pore space, a level of detail not usually retained when constructing the pore network geometry. For this reason, snap-off has been captured by rule-based algorithms that rely on simple geometric terms such as angularity of the chosen pore elements (Hughes and Blunt 2000).

3.4.2 Dynamic Algorithms

The terminology *dynamic network model* has come to signify the class of multiphase flow algorithms that accounts for viscous effects. The differences between quasi-static and dynamic models are quite dramatic, including the algorithms, computational demands, and applications. To understand their importance, consider that viscous effects are intrinsic to behaviors such spontaneous imbibition, viscous fingering, wetting film drainage, blob mobilization, or modeling time-dependent behavior in any flow process.

Dynamic multiphase flow algorithms have been evolving for more than 30 years, yet research remains active and no single approach has become the standard. Reasons include similar challenges seen with direct methods and quasi-static modeling (e.g., computational demands and accounting for the positions of fluid interfaces), as well as other issues such as the introduction of non-smooth functions into the equations, which makes the numerical solutions less stable.

Since no current model can account for all effects important for multiphase flow, a researcher new to this area will need to decide what functionalities are most important versus what can be neglected for a given application. For example, while wettability effects such as spatial variation in contact angle and/or contact angle hysteresis can be included if needed, many models assume a uniformly wetting material to help make the interface computations more tractable.

Many dynamic methods (and variants within methods) have been developed, which makes classification a challenge. Here, we summarize three broad techniques that have each proved effective in multiple implementations and applications.

The first category includes models that decouple the capillary pressure and the viscous pressure in the dynamic part of the algorithm (Blunt and King 1991; Hughes and Blunt 2000; Knudsen et al. 2002; Nguyen et al. 2006; Idowu and Blunt 2010; Ramstad et al. 2009). Numerically, this can be thought of as an explicit time-stepping approach: viscous effects are computed using the current pore-scale distribution of phases from a quasi-steady flow computation; the resulting pressure field is then compared against criteria for invasion, retraction, or snap-off events everywhere a fluid–fluid interface is present, and local fluid displacements are made accordingly. Timestep size is usually dictated by the time required to achieve one or more filling events. The main advantage is computational efficiency, although most authors also provide corresponding physical assumptions, for instance, zero capillary pressure difference in pores (Blunt and King 1991; Nordhaug et al. 2003), pore throats fully

occupied by one or the other of the two phases (Blunt and King 1991), two phases allowed in pore throats but only for corner flow (Bakke and Øren 1997), or neglecting viscosity of the displaced non-wetting phase during imbibition (Hughes and Blunt 2000).

The second class of dynamic algorithms is referred to as the Washburn or the single-pressure approach. These models are based on the same conservation equation presented for single-phase flow (Eq. 22), but the pore-throat flow rate term is written to account for the possibility of interface(s) in the pore throat:

$$Q_{1,2} = -g_{1,2}\frac{p_2 - p_1 - \Delta p_{c_{1,2}}}{l_{1,2}}. \tag{26}$$

This equation is the same as Eq. (21) except for the added term $\Delta p_{c_{1,2}}$, which is the capillary pressure drop across interface(s) when two fluids are present in a series configuration in throat 1,2. The numerical role of this extra pressure drop is to determine whether the interface is advancing, retracting, or static during a current timestep. Since $\Delta p_{c_{1,2}}$ depends on the local geometry (and interfacial tension and contact angle), and since p_1 and p_2 depend on the overall network solution, this approach couples the viscous and capillary effects in a way that the first approach does not. The system of equations is nonlinear and therefore presents greater computational challenges in terms of both speed and stability.

The Washburn approach was used by Koplik and Lasseter (1985), who are usually credited with the first dynamic network model, and shortly thereafter by Dias and Payatakes (1986) and Lenormand et al. (1988), each with a unique implementation for the processes being studied. Since that time, numerous other researchers have employed this approach including (Mogensen and Stenby 1998; Aker et al. 1998; Dahle and Celia 1999; Singh and Mohanty 2003; Knudsen et al. 2002; Ramstad and Hansen 2006).

A third more recent approach is to write independent mass conservation equations for each phase (for every pore). For incompressible fluids, Eq. (22) becomes

$$\sum_j Q_{i,j}^{\alpha} = \frac{\partial V_i^{\alpha}}{\partial t} \quad \text{or} \quad \sum_j Q_{i,j}^{\alpha} = V_i \frac{\partial S_i^{\alpha}}{\partial t}, \tag{27}$$

where α represents the fluid phase, which for this discussion of two-phase flow is generally written as wetting (w) and non-wetting (nw), and S_i^{α} is the non-dimensional volume fraction (saturation) in each pore. Pore-throat flow rates are written as in Eq. (21) but separately for each phase:

$$Q_{1,2}^{w} = -g_{1,2}^{w}\frac{p_2^{w} - p_1^{w}}{l_{1,2}} \quad \text{and} \quad Q_{1,2}^{nw} = -g_{1,2}^{nw}\frac{p_2^{nw} - p_1^{nw}}{l_{1,2}}. \tag{28}$$

This approach produces two equations per pore, which are then coupled through the saturation constraint $S_i^{w} + S_i^{nw} = 1$ and pore capillary pressure equations $p_i^{nw} = p_i^{w} + p_{c,i}(S_i^{w})$.

The key to making this approach work is the ability to compute pore capillary pressures $p_{c,i}(S_i^{w})$ and pore-throat conductances $g_{i,j}^{\alpha}$. These computations involve the same difficulties described above: keeping track of interface locations, calculating interface geometries to obtain local capillary pressures, and reflecting critical events such as invasion, retraction, and snap off in the parameters $g_{i,j}^{w}$ and $g_{i,j}^{nw}$.

If these parameters can be computed during dynamic simulations, then this technique has a number of advantages. It is a more direct representation of the conservation laws and pore-scale physics (reducing rule-based decisions), the two-pressure formulation naturally allows for modeling both parallel flow and series interfaces in pore throats (as well as capillary pressure gradients), and the same algorithm can be solved using explicit, semi-implicit,

or fully implicit schemes, depending the desired balance between efficiency, stability, and accuracy.

This formulation for dynamic modeling has been used to study spontaneous imbibition (Thompson 2002), non-equilibrium capillary pressure relationships (Joekar-Niasar et al. 2010), steady-state two-phase flow and relative permeability (Sheng and Thompson 2016), and fingering of air into water saturated porous media (Sweijen et al. 2018).

4 Applications of Pore-Scale Modeling

Porous media are abundant in nature and appear over all length scales. On larger scales, multiphase flow in porous media is mainly treated through a phenomenological extension of Darcy's equation that describes a linear relationship between flow rate and viscous pressure drop (Darcy 1856)

$$\mathbf{q} = -\frac{k_r k}{\mu} \nabla p. \tag{29}$$

The absolute permeability k is a material property of the structure of the pore space itself (Berg 2014). The relative permeability k_r is a constitutive relation that comes from an averaging of the relationship between fluid phases that flow through the pore space. Both quantities need to be established by interpreting pore-scale flow either from experiments or from simulations. Only for very simple pore spaces can these properties be determined analytically.

Both absolute and relative permeability are inputs for simulation of fluid flow on larger scales. When pore-scale modeling is conducted to populate larger-scale models with, for example, absolute and relative permeability values, the pore-scale models need to be large enough for the calculated values to be representative for the material that is modeled, i.e., they need to cover a representative elementary volume (REV) (Bear 1988; Nordahl and Ringrose 2008). The size of a REV is linked to the heterogeneity of the material and to the transport process: The absolute permeability of a periodic material like a cubic pack of equal spheres will have a REV consisting of the periodic unit cell of size comparable to the spheres. The absolute permeability of fairly homogeneous granular material might need at least 10 grains in each direction. Strongly heterogeneous materials, multiphase flow, and solute dispersion demand even larger REV.

In the early years, pore-scale modeling was restricted by imaging and computational capacities, and algorithms for simulation of multiphase flow were limited. Due to limitations in imaging capabilities, early pore-scale modeling dealt mostly with artificial or 3D porous media reconstructed from 2D cross sections (Adler et al. 1990). While 2D cross sections probably will remain superior when it comes to resolution and coverage, present-day 3D imaging produces samples at the limit of our computational power (Andrä et al. 2013; Wildenschild and Sheppard 2013). This has reduced the need for 2D-to-3D reconstruction algorithms.

Due to computational efficiency, multiphase simulations first started with network simulations (Fatt 1956; Jerauld and Salter 1990; Blunt and King 1991; Bakke and Øren 1997). Simulations directly on 3D representations of the pore structure started with a focus on single-phase transport properties due to curbs in computing power and a lack of available algorithms (Roberts and Schwartz 1985; Higuera and Succi 1989; Adler et al. 1992; Schwartz et al. 1994; Ferreol and Rothman 1995). However, such single-phase simulations unlocked one of the advantages of pore-scale modeling; obtaining effective transport properties on the same pore structure, and thereby well-defined cross-property relations linked to pore-structure characteristics (Schwartz et al. 1993; Arns et al. 2005; Berg and Held 2016).

Fatt pioneered pore-scale simulations with his pore-scale network modeling (Fatt 1956). His papers were published in the Petroleum Transactions of AIME, and in the half century since the work of Fatt, hydrocarbon extraction has been a driver of pore-scale modeling on a number of fronts. One objective has been fundamental understanding of flow in porous media: As an example, theories on the relation between capillary pressure, saturation and interfacial area (Hassanizadeh and Gray 1993) has been investigated both numerically (Held and Celia 2001) and through imaging (Culligan et al. 2004). Fast 3D imaging enables the visualization of movement of the fluid interfaces inside the porous medium. While the time resolution is insufficient to capture the fluid interface movement during a Haines jump, it is fine enough to describe the start and end states of such a jump (Berg et al. 2013). Pore-scale information on interface movement and ganglion flow gives a broader description of multiphase flow (Datta et al. 2014; Youssef et al. 2014).

Another objective for reservoir characterization has been pore-scale modeling as an extension or replacement of special core analysis in traditional workflows for reservoir simulation. Pore-scale modeling provides similar data as conventional and special core analysis. It therefore enters subsurface workflows at the same point as the mentioned laboratory data (Berg et al. 2017).

For samples of decent reservoir quality, traditional experiments for conventional core analysis data, such as porosity, absolute permeability and conductivity, are fast, relatively cheap, and fairly reliable. This lowers the incentives for pore-scale modeling for such data types. The next step of complexity in pore-scale modeling is primary drainage, where invasion percolation type of simulations has proven to be predictable and robust. Thus, pore-scale modeling of primary drainage capillary pressure and resistivity index is computationally easy and produce reliable results. Pore-scale modeling for petrophysical properties and primary drainage data has been documented as valuable (Fredrich et al. 2014). In addition, simulations can be used for sensitivity testing and to reduce uncertainty in flow parameters. This is useful for applications to more complex fluids and gases, like CO_2 (Blunt 2017), that can be challenging to handle in experiments.

Pore-scale modeling of multiphase flow properties is less robust and more computationally intensive. Among other reasons, this is due to the complex nature of wettability and the lack of resolution to capture film flow. Still, pore-scale modeling has been recognized as a valuable tool, mainly due to the reduced time for data acquisition (Berg et al. 2017).

4.1 Direct Modeling Versus Network Modeling

This review has presented two methods for pore-scale modeling: a direct method (LBM) and pore-network modeling. These two methods are quite different, each with strengths and weaknesses. However, these differences also make them highly complementary, with one or the other types of method usually being more appropriate for a given modeling or research problem.

Direct models are the more rigorous approach, based on numerical solution of the equations of motion within the actual pore geometry (to the resolution that a digital image or gridding scheme allows). The resulting solution includes the full velocity and pressure fields, meaning that one can resolve velocity distributions and velocity gradients within pores, and compute and track continuous streamlines for Lagrangian modeling. The main disadvantage of all direct approaches is the heavy computational demand, which limits the size of models. This paper focuses on LBM in particular, which has become the most widely used direct method for pore-scale modeling. Advantages include its automatic handling of solid/fluid and fluid/fluid interfaces, and its amenability to parallelization for improved computational performance.

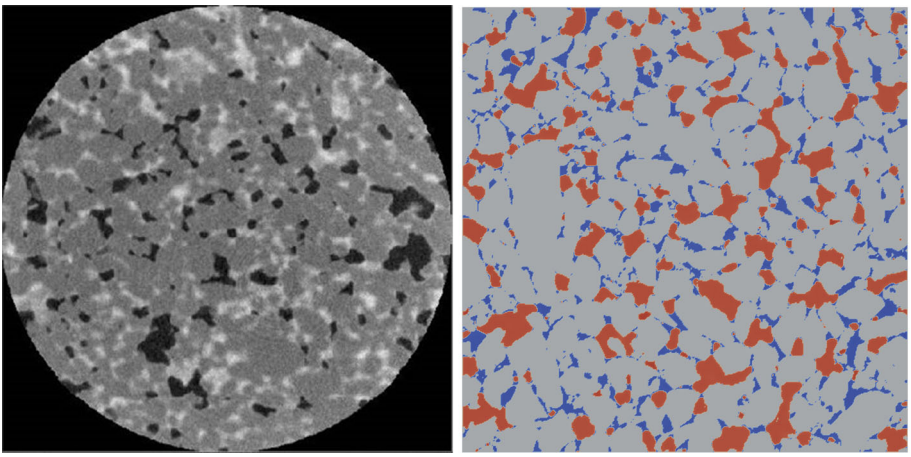

Fig. 5 The left image shows a micro-CT image of a core sample containing two distinguishable fluids; oil as black and water as light gray. The right image shows the fluid distribution from a LBM simulation. Both images are courtesy of Equinor ASA

In contrast to direct methods, pore-network models involve significant approximations to both geometry and transport: the detailed pore-space geometry is simplified to an interconnected network of pores and pore throats, and for fluid transport the model employs a set of simultaneous but independent Poiseuille flow problems (i.e., with boundary position that are single-point pressures in each pore; modeling of other transport process have analogous simplifications). Consequently, pore-network modeling allows for computation of flow rates at the pore scale, but not sub-pore-scale velocity distributions or calculation of continuous streamlines through the porous media. These limitations are balanced by significant benefits, two of the foremost being dramatic computational savings (faster solution and/or much larger physical domains) and modeling that is freed from the resolution limitations associated with a grid or mesh.

The remainder of this section elaborates on key differences between direct and pore-network modeling and implications for the algorithms and/or the model predictions.

Digital pore-scale images, from, for example, X-ray computed tomography (CT), can be used directly as input grids to LBM simulations. As an example, Fig. 5 shows that multiphase LBM is able reproduce an in situ fluid distributions. For much the same reasons mentioned above that network models cannot resolve sub-pore-scale flow fields, this level of detailed (quantitative) information about fluid distributions is not possible.

For direct modeling, the pores must be resolved by enough voxels to accommodate a correct flow profile. Therefore, the main flow paths need to be properly resolved, while resolving pore space with slow flow can be less important, depending on the application. In both direct and network modeling, sub-resolution porosity can be captured by introducing a third phase in addition to the resolved porosity and matrix. The unresolved porosity will have significant contribution to porosity but insignificant contribution to fluid flow and is typically assumed to always contain water. The unresolved porosity can have significant contribution to other transport properties such as diffusion and electrical conductance.

In network modeling, fluid–fluid interfaces are treated as volume-free surfaces, and wettability is implemented through contact angles with the network elements. For direct modeling, the fluid–fluid interface widths must be relatively sharp, with a correct fluid–solid wettability interaction. This is an issue when treating creeping film flows near boundaries, and prevent-

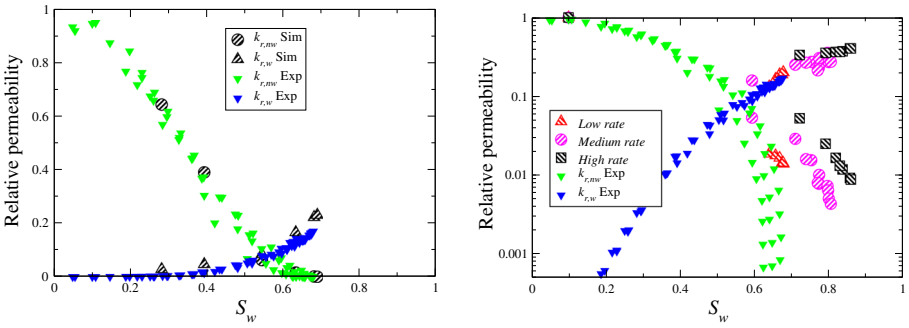

Fig. 6 Steady-state (left) versus unsteady state (right) relative permeability curves for a digital Berea model. The experimental data are taken from Oak et al. (1990) and show steady-state water flooding. The figure is adapted from Ramstad et al. (2012)

ing too-large diffusivity in immiscible transport (Liu et al. 2016). Due to the scale difference between bulk and film flow, capturing both bulk and film flow at the same time as capturing a representative volume is computationally challenging. For direct modeling, this has been remedied by including special boundary conditions at the solid walls to maintain unresolved films (Nie et al. 2016).

As pore-network models are a simplified abstraction of the underlying pore structure and flow patterns, they tend to be computationally lighter than direct modeling. Fortunately, the LBM is straightforward to run in parallel since the collision is done locally. It has an explicit time scheme and scales well on multiple processors. With current computational capacity and parallel implementations, multiphase LBM can be simulated on sample sizes comparable to typical sizes of micro-CT images, thereby capturing enough pore bodies to constitute a representative volume. General-purpose GPU implementations have been investigated for LBM (Tölke 2010; McClure et al. 2010). This approach has limitations related to memory constraints on GPUs, but has otherwise shown to increase computational efficiency significantly.

Both dynamic network models and the LBM method can model how viscous and capillary forces affect two-phase flow, e.g., relative permeability at different flow rates shown in Fig. 6. However, they are best suited for flow regimes where viscous forces contribute to the overall flow. For LBM simulations, timesteps are small when treating pore-scale dynamics. This is a direct consequence of the scaling of physical quantities as described in Sect. 2.3.3. Hence, smaller lattice constants will lead to smaller timesteps to scale physical quantities correctly. Dynamic network models have similar issues. As a consequence, simulations may become computationally heavy.

For LBM use in multiphase pore-scale simulations on complex and natural porous media, one of the largest issues and limitations relates to the spurious currents near fluid–fluid and fluid–solid interfaces. The magnitude of the spurious currents scale with the local force field near fluid interfaces [see Eq. (12)]. Hence, they are most profound for low flow rates and high interfacial tensions. Spurious currents tend to average to zero over a representative volume, but in scenarios with low overall flow rates they may cause noise and even unphysical results for hydrodynamic quantities. In addition, if the local velocity of the spurious currents become too large, numerical stability issues may arise.

In completely capillary-dominated regimes, e.g., where the flow rate is very low, fluctuations and noise could make both dynamic network models and LBM inadequate. Such capillary-dominated flow regimes are well suited for quasi-static network models. Quasi-static network models tend to be more stable and computational light than dynamic network

models and direct grid-based solvers. Flow rates away from wells in a reservoir is in the order of meter per day, so for most reservoir fluids this yields capillary-dominated flow.

As outlined above, the applied simulation method is dependent on the desired outcome. Grid-based methods like LBM honor the digitized pore structure and viscous forces. For dynamic network models, the pore structure is simplified; however, such network models treat fluid–fluid interfaces as surfaces and are therefore well suited for capturing small-scale features like film flow. Quasi-static network models ignore viscous forces; however, they are well suited to capture capillary-dominated flow regimes and are more efficient computationally than the previous mentioned methods. The service providers of digital rock technology have tended to specialize in either grid-based or network modeling methods.

5 Summary

This article has presented the basic background for popular pore-scale simulation methods and their applications. The two main sections of the article reflect two distinct approaches to pore-scale modeling: direct simulations on grid models of the pore space and simulations on network representations.

Direct simulations keep the imaged geometry of the pore space. They are preferable whenever they are able to properly represent the transport process and at the same time are computationally feasible. This is fulfilled for both single-phase fluid flow and electrical conductivity, and thus, direct simulation is the recommended method for these properties.

In this article, the direct simulation approach was illustrated by the lattice Boltzmann method. Arguably, this is the most popular method for simulation of fluid flow at the pore scale. Different relaxation methods were discussed; the multiple relaxation method yields more flexibility but with the cost of a more complex simulation model. For the multiphase methods, several phase separation methods were presented and their strengths and weaknesses were discussed: the color gradient method gives sharp interfaces, while inter-particle methods such as Shan–Chen has a more physical representation of the phase separation.

While direct simulation is the preferred method for single-phase flow simulations, it has several drawbacks with respect to multiphase flow: It is computational heavy, it needs a high resolution to capture film flow, and the different time scales associated with different pore filling events are difficult to capture with the time-stepping scheme.

Network models are well suited to represent film flow. Capillary-dominated flow modeled by quasi-static methods is computationally very efficient. Dynamic network models able to capture viscous effects are important but can increase computational cost considerably.

Applications, implementation and comparison of pore-scale simulations were presented in the last section of this article. The applied pore-scale simulation method is highly dependent on the transport problem, as discussed above. Successful implementations of pore-scale simulations into typical core analysis workflows were referenced as an example of modern application.

Pore-scale simulation of transport in porous media is widespread. It has been relatively successful in predictive modeling of transport processes, and where more traditional experimental procedures are challenging. At the same time, such simulations have the ability to reveal the pore-scale causes for the effective properties, thereby yielding a deeper understanding of the transport processes. Such pore-scale understanding can be important for correct modeling of large-scale transport phenomena.

With the advancement in pore-scale imaging techniques such as micro-CT, the in situ fluid distributions in real porous media can be obtained (Berg et al. 2013). In the near future, it

is expected that integrated imaging and simulation techniques will provide valuable insight in pore-scale flow mechanisms. It is therefore fair to assume that simulations of complex transport directly on images of porous media will continue to attract much attention in the years to come.

Acknowledgements The authors would like to thank Equinor ASA for granting permission to publish this paper. The authors thank Anders Torland for Fig. 4, and Anders Kristoffersen, Karen Melhuus, and Lars Rennan (Equinor) for providing micro-CT images of flooding experiments. Thomas Ramstad thanks Kristian Sandengen and Knut Uleberg for helpful discussions and comments. Carl Fredrik Berg acknowledges support from the Research Council of Norway through its Centre of Excellence funding scheme with Project No. 262644.

References

Adler, P.M., Jacquin, C.G., Quiblier, J.A.: Flow in simulated porous media. Int. J. Multiph. Flow **16**(4), 691–712 (1990)

Adler, P.M., Jacquin, C.G., Thovert, J.F.: The formation factor of reconstructed porous media. Water Resour. Res. **28**(6), 1571–1576 (1992)

Akai, T., Bijeljic, B., Blunt, M.J.: Wetting boundary condition for the color-gradient lattice Boltzmann method: validation with analytical and experimental data. Adv. Water Resour. (2018)

Aker, E., Måløy, K.J., Hansen, A., Batrouni, G.G.: A two-dimensional network simulator for two-phase flow in porous media. Transp. Porous Media **32**(2), 163–186 (1998)

Anderson, W.G.: Wettability literature survey part 5: the effects of wettability on relative permeability. J. Pet. Technol. **39**(11), 1–453 (1987)

Andrä, H., Combaret, N., Dvorkin, J., Glatt, E., Han, J., Kabel, M., Keehm, Y., Krzikalla, F., Lee, M., Madonna, C.: Digital rock physics benchmarks—Part II: computing effective properties. Comput. Geosci. **50**, 33–43 (2013)

Arns, C.H., Knackstedt, M.A., Martys, N.S.: Cross-property correlations and permeability estimation in sandstone. Phys. Rev. E **72**(4), 046,304 (2005). https://doi.org/10.1103/PhysRevE.72.046304

Bakke, S., Øren, P.E., et al.: 3-D pore-scale modelling of sandstones and flow simulations in the pore networks. Spe J. **2**(02), 136–149 (1997)

Bear, J.: Dynamics of Fluids in Porous Media. Dover, NY (1988)

Berg, C.F.: Permeability description by characteristic length, tortuosity, constriction and porosity. Transp. Porous Media **103**(3), 381–400 (2014)

Berg, C.F., Held, R.: Fundamental transport property relations in porous media incorporating detailed pore structure description. Transp. Porous Media **112**(2), 467–487 (2016)

Berg, C.F., Lopez, O., Berland, H.: Industrial applications of digital rock technology. J. Pet. Sci. Eng. **157**, 131–147 (2017)

Berg, S., Ott, H., Klapp, S.A., Schwing, A., Neiteler, R., Brussee, N., Makurat, A., Leu, L., Enzmann, F., Schwarz, J.O.: Real-time 3D imaging of Haines jumps in porous media flow. Proc. Natl. Acad. Sci. **110**(10), 3755–3759 (2013)

Bhatnagar, P.L., Gross, E.P., Krook, M.: A model for collision processes in gases. I. Small amplitude processes in charged and neutral one-component systems. Phys. Rev. **94**(3), 511 (1954)

Blunt, M., King, P.: Relative permeabilities from two-and three-dimensional pore-scale network modelling. Transp. Porous Media **6**(4), 407–433 (1991)

Blunt, M., Scher, H.: Pore-level modeling of wetting. Phys. Rev. E **52**(6, B), 6387–6403 (1995). https://doi.org/10.1103/PhysRevE.52.6387

Blunt, M.J.: Multiphase Flow in Permeable Media: A Pore-Scale Perspective. Cambridge University Press, Cambridge (2017)

Blunt, M.J., Bijeljic, B., Dong, H., Gharbi, O., Iglauer, S., Mostaghimi, P., Paluszny, A., Pentland, C.: Pore-scale imaging and modelling. Adv. Water Resour. **51**, 197–216 (2013)

Bryant, S., Blunt, M.: Prediction of relative permeability in simple porous media. Phys. Rev. A **46**(4), 2004 (1992)

Bryant, S.L., King, P.R., Mellor, D.W.: Network model evaluation of permeability and spatial correlation in a real random sphere packing. Transp. Porous Media **11**(1), 53–70 (1993)

Buick, J., Greated, C.: Gravity in a lattice Boltzmann model. Phys. Rev. E **61**(5), 5307 (2000)

Bultreys, T., De Boever, W., Cnudde, V.: Imaging and image-based fluid transport modeling at the pore scale in geological materials: a practical introduction to the current state-of-the-art. Earth-Sci. Rev. **155**, 93–128 (2016)
Chandler, R., Koplik, J., Lerman, K., Willemsen, J.F.: Capillary displacement and percolation in porous media. J. Fluid Mech. **119**, 249–267 (1982)
Chapman, S., Cowling, T.: The Mathematical Theory of Non-uniform Gases: An Account of the Kinetic Theory of Viscosity, Thermal Conduction and Diffusion in Gases. Cambridge Mathematical Library. Cambridge University Press, Cambridge (1970)
Chatzis, I., Dullien, F.A., et al.: Modelling pore structure by 2-D and 3-D networks with applicationto sandstones. J. Can. Pet. Technol. **16**(01) (1977)
Chen, Jd, Koplik, J.: Immiscible fluid displacement in small networks. J. Colloid Interface Sci. **108**(2), 304–330 (1985)
Chen, S., Doolen, G.D.: Lattice Boltzmann method for fluid flows. Annu. Rev. Fluid Mech. **30**(1), 329–364 (1998)
Connington, K., Lee, T.: A review of spurious currents in the lattice Boltzmann method for multiphase flows. J. Mech. Sci. Technol. **26**(12), 3857–3863 (2012)
Culligan, K.A., Wildenschild, D., Christensen, B.S.B., Gray, W.G., Rivers, M.L., Tompson, A.F.B.: Interfacial area measurements for unsaturated flow through a porous medium. Water Resour. Res. **40**(12) (2004). https://doi.org/10.1029/2004WR003278
Dahle, H.K., Celia, M.A.: A dynamic network model for two-phase immiscible flow. Comput. Geosci. **3**(1), 1–22 (1999)
Darcy, H.: Les fontaines publiques de la ville de Dijon: exposition et application... Victor Dalmont (1856)
Datta, S.S., Dupin, J.B., Weitz, D.A.: Fluid breakup during simultaneous two-phase flow through a three-dimensional porous medium. Phys. Fluids **26**(6), 062,004 (2014)
d'Humières, D.: Multiple–relaxation–time lattice Boltzmann models in three dimensions. Philos. Trans. R. Soc. Lond. Ser. A: Math. Phys. Eng. Sci. **360**(1792), 437–451 (2002)
Dias, M., Payatakes, A.: Network models for 2-phase flow in porous media. 1. Immiscible microdisplacement of nonwetting fluids. J. Fluid Mech. **164**, 305–336 (1986). https://doi.org/10.1017/S0022112086002574
Fatt, I.: The network model of porous media (1956)
Ferreol, B., Rothman, D.H.: Lattice-Boltzmann simulations of flow through Fontainebleau sandstone. In: Multiphase Flow in Porous Media, pp. 3–20. Springer, Berlin (1995)
Fredrich, J.T., Lakshtanov, D.L., Lane, N.M., Liu, E.B., Natarajan, C.S., Ni, D.M., Toms, J.J.: Digital rocks: developing an emerging technology through to a proven capability deployed in the business. Society of Petroleum Engineers (2014). https://doi.org/10.2118/170752-MS
Ginzbourg, I., Adler, P.: Boundary flow condition analysis for the three-dimensional lattice Boltzmann model. J. de Phys. II **4**(2), 191–214 (1994)
Ginzburg, I., Verhaeghe, F., d'Humieres, D.: Two-relaxation-time lattice boltzmann scheme: about parametrization, velocity, pressure and mixed boundary conditions. Commun. Comput. Phys. **3**(2), 427–478 (2008)
Grunau, D., Chen, S., Eggert, K.: A lattice Boltzmann model for multiphase fluid flows. Phys. Fluids A: Fluid Dyn. **5**(10), 2557–2562 (1993)
Gunstensen, A.K., Rothman, D.H., Zaleski, S., Zanetti, G.: Lattice Boltzmann model of immiscible fluids. Phys. Rev. A **43**(8), 4320 (1991)
Guo, Z., Shu, C.: Lattice Boltzmann Method and Its Applications in Engineering, vol. 3. World Scientific, Singapore (2013)
Guo, Z., Zheng, C., Shi, B.: Discrete lattice effects on the forcing term in the lattice boltzmann method. Phys. Rev. E **65**(4), 046,308 (2002)
Hassanizadeh, S.M., Gray, W.G.: Thermodynamic basis of capillary pressure in porous media. Water Resour. Res. **29**(10), 3389–3407 (1993)
He, X., Chen, S., Zhang, R.: A lattice boltzmann scheme for incompressible multiphase flow and its application in simulation of Rayleigh–Taylor instability. J. Comput. Phys. **152**(2), 642–663 (1999)
Hecht, M., Harting, J.: Implementation of on-site velocity boundary conditions for d3q19 lattice Boltzmann simulations. J. Stat. Mech.: Theory Exp. **2010**(01), P01,018 (2010)
Held, R.J., Celia, M.A.: Modeling support of functional relationships between capillary pressure, saturation, interfacial area and common lines. Adv. Water Resour. **24**(3–4), 325–343 (2001)
Higuera, F., Succi, S.: Simulating the flow around a circular cylinder with a lattice boltzmann equation. EPL (Europhysics Letters) **8**(6), 517 (1989)
Huang, H., Thorne Jr., D.T., Schaap, M.G., Sukop, M.C.: Proposed approximation for contact angles in Shan-and-Chen-type multicomponent multiphase lattice Boltzmann models. Phys. Rev. E **76**(6), 066,701 (2007)

Hughes, R.G., Blunt, M.J.: Pore scale modeling of rate effects in imbibition. Transp. Porous Media **40**(3), 295–322 (2000). https://doi.org/10.1023/A:1006629019153
Idowu, N.A., Blunt, M.J.: Pore-scale modelling of rate effects in waterflooding. Transp. Porous Media **83**(1, SI), 151–169 (2010). https://doi.org/10.1007/s11242-009-9468-0
Jerauld, G.R., Salter, S.J.: The effect of pore-structure on hysteresis in relative permeability and capillary pressure: pore-level modeling. Transp. Porous Media **5**(2), 103–151 (1990)
Jettestuen, E., Helland, J.O., Prodanović, M.: A level set method for simulating capillary-controlled displacements at the pore scale with nonzero contact angles. Water Resour. Res. **49**(8), 4645–4661 (2013)
Jin, G., Patzek, T.W., Silin, D.B., et al.: Direct prediction of the absolute permeability of unconsolidated and consolidated reservoir rock. In: SPE Annual Technical Conference and Exhibition. Society of Petroleum Engineers (2004)
Joekar-Niasar, V., Hassanizadeh, S.: Analysis of fundamentals of two-phase flow in porous media using dynamic pore-network models: a review. Crit. Rev. Environ. Sci. Technol. **42**(18), 1895–1976 (2012)
Joekar-Niasar, V., Hassanizadeh, S.M., Dahle, H.K.: Non-equilibrium effects in capillarity and interfacial area in two-phase flow: dynamic pore-network modelling. J. Fluid Mech. **655**, 38–71 (2010). https://doi.org/10.1017/S0022112010000704
Knudsen, H.A., Aker, E., Hansen, A.: Bulk flow regimes and fractional flow in 2d porous media by numerical simulations. Transp. Porous Media **47**(1), 99–121 (2002)
Koplik, J.: Creeping flow in two-dimensional networks. J. Fluid Mech. **119**, 219–247 (1982)
Koplik, J., Lasseter, T., et al.: Two-phase flow in random network models of porous media. Soc. Pet. Eng. J. **25**(01), 89–100 (1985)
Koroteev, D., Dinariev, O., Evseev, N., Klemin, D., Nadeev, A., Safonov, S., Gurpinar, O., Berg, S., van Kruijsdijk, C., Armstrong, R., et al.: Direct hydrodynamic simulation of multiphase flow in porous rock. Petrophysics **55**(04), 294–303 (2014)
Latt, J., Chopard, B.: Lattice Boltzmann method with regularized pre-collision distribution functions. Math. Comput. Simul. **72**(2–6), 165–168 (2006)
Latva-Kokko, M., Rothman, D.H.: Diffusion properties of gradient-based lattice Boltzmann models of immiscible fluids. Phys. Rev. E **71**(5), 056,702 (2005)
Latva-Kokko, M., Rothman, D.H.: Static contact angle in lattice Boltzmann models of immiscible fluids. Phys. Rev. E **72**(4), 046,701 (2005)
Leclaire, S., Parmigiani, A., Malaspinas, O., Chopard, B., Latt, J.: Generalized three-dimensional lattice boltzmann color-gradient method for immiscible two-phase pore-scale imbibition and drainage in porous media. Phys. Rev. E **95**(3), 033,306 (2017)
Lenormand, R., Touboul, E., Zarcone, C.: Numerical-models and experiments on immiscible displacements in porous-media. J. Fluid Mech. **189**, 165–187 (1988). https://doi.org/10.1017/S0022112088000953
Lenormand, R., Zarcone, C., Sarr, A.: Mechanisms of the displacement of one fluid by another in a network of capillary ducts. J. Fluid Mech. **135**, 337–353 (1983)
Lenormand, R., Zarcone, C., et al.: Role of roughness and edges during imbibition in square capillaries. In: SPE Annual Technical Conference and Exhibition. Society of Petroleum Engineers (1984)
Li, Q., Luo, K.H., Kang, Q., He, Y., Chen, Q., Liu, Q.: Lattice boltzmann methods for multiphase flow and phase-change heat transfer. Prog. Energy Combust. Sci. **52**, 62–105 (2016)
Liang, Z., Ioannidis, M., Chatzis, I.: Geometric and topological analysis of three-dimensional porous media: pore space partitioning based on morphological skeletonization. J. Colloid Interface Sci. **221**(1), 13–24 (2000)
Lindquist, W.B., Lee, S.M., Coker, D.A., Jones, K.W., Spanne, P.: Medial axis analysis of void structure in three-dimensional tomographic images of porous media. J. Geophys. Res.: Solid Earth **101**(B4), 8297–8310 (1996)
Liu, H., Kang, Q., Leonardi, C.R., Schmieschek, S., Narváez, A., Jones, B.D., Williams, J.R., Valocchi, A.J., Harting, J.: Multiphase lattice Boltzmann simulations for porous media applications. Comput. Geosci. **20**(4), 777–805 (2016)
Manwart, C., Aaltosalmi, U., Koponen, A., Hilfer, R., Timonen, J.: Lattice-Boltzmann and finite-difference simulations for the permeability for three-dimensional porous media. Phys. Rev. E **66**(1), 016,702 (2002)
Martys, N.S., Chen, H.: Simulation of multicomponent fluids in complex three-dimensional geometries by the lattice Boltzmann method. Phys. Rev. E **53**(1), 743 (1996)
Mason, G.: A model of the pore space in a random packing of equal spheres. J. Colloid Interface Sci. **35**(2), 279–287 (1971)
Mason, G., Morrow, N.R.: Capillary behavior of a perfectly wetting liquid in irregular triangular tubes. J. Colloid Interface Sci. **141**(1), 262–274 (1991)
Mayer, R.P., Stowe, R.A.: Mercury porosimetry—breakthrough pressure for penetration between packed spheres. J. Colloid Sci. **20**(8), 893–911 (1965)

Mazloomi, M,A., Chikatamarla, S.S., Karlin, I.V.: Entropic lattice Boltzmann method for multiphase flows. Phys. Rev. Lett. **114**, 174,502 (2015). https://doi.org/10.1103/PhysRevLett.114.174502
McClure, J.E., Prins, J.F., Miller, C.T.: Comparison of CPU and GPU implementations of the lattice Boltzmann method. In: XVIII International Conference on Computational Methods in Water Resources (2010)
McNamara, G.R., Zanetti, G.: Use of the Boltzmann equation to simulate lattice-gas automata. Phys. Rev. Lett. **61**(20), 2332 (1988)
Mogensen, K., Stenby, E.: A dynamic two-phase pore-scale model of imbibition. Transp. Porous Media **32**(3), 299–327 (1998). https://doi.org/10.1023/A:1006578721129
Nguyen, V.H., Sheppard, A.P., Knackstedt, M.A., Val Pinczewski, W.: The effect of displacement rate on imbibition relative permeability and residual saturation. J. Pet. Sci. Eng. **52**(1–4), 54–70 (2006). https://doi.org/10.1016/j.petrol.2006.03.020
Nie, X., Gundepalli, V., Mu, Y., Sungkorn, R., Toelke, J.: Numerical investigation of oil-water drainage and imbibition in digitized sandstones. Mech. Ind. **17**(2), 202 (2016)
Nordahl, K., Ringrose, P.S.: Identifying the representative elementary volume for permeability in heterolithic deposits using numerical rock models. Math. Geosci. **40**(7), 753–771 (2008)
Nordhaug, H., Celia, M., Dahle, H.: A pore network model for calculation of interfacial velocities. Adv. Water Resour. **26**(10), 1061–1074 (2003). Fluid-fluid interfaces;
Oak, M., Baker, L., Thomas, D., et al.: Three-phase relative permeability of Berea sandstone. J. Pet. Technol. **42**(08), 1–054 (1990)
Øren, P., Bakke, S., Arntzen, O.J.: Extending predictive capabilities to network models. SPE J. **3**(04), 324–336 (1998)
Pan, C., Luo, L.S., Miller, C.T.: An evaluation of lattice Boltzmann schemes for porous medium flow simulation. Comput. Fluids **35**(8–9), 898–909 (2006)
Payatakes, A.: Dynamics of oil ganglia during immiscible displacement in water-wet porous media. Annu. Rev. Fluid Mech. **14**(1), 365–393 (1982)
Premnath, K.N., Abraham, J.: Three-dimensional multi-relaxation time (MRT) lattice-Boltzmann models for multiphase flow. J. Comput. Phys. **224**(2), 539–559 (2007)
Princen, H.M.: Capillary phenomena in assemblies of parallel cylinders: I. Capillary rise between two cylinders. J. Colloid Interface Sci. **30**(1), 69–75 (1969)
Princen, H.M.: Capillary phenomena in assemblies of parallel cylinders: II. Capillary rise in systems with more than two cylinders. J. Colloid Interface Sci. **30**(3), 359–371 (1969)
Princen, H.M.: Capillary phenomena in assemblies of parallel cylinders: III. Liquid columns between horizontal parallel cylinders. J. Colloid Interface Sci. **34**(2), 171–184 (1970)
Raeini, A.Q., Blunt, M.J., Bijeljic, B.: Modelling two-phase flow in porous media at the pore scale using the volume-of-fluid method. J. Comput. Phys. **231**(17), 5653–5668 (2012)
Ramstad, T., Hansen, A.: Cluster evolution in steady-state two-phase flow in porous media. Phys. Rev. E **73**(2), 026,306 (2006)
Ramstad, T., Hansen, A., Øren, P.E.: Flux-dependent percolation transition in immiscible two-phase flows in porous media. Phys. Rev. E **79**(3), 036,310 (2009)
Ramstad, T., Idowu, N., Nardi, C., Øren, P.E.: Relative permeability calculations from two-phase flow simulations directly on digital images of porous rocks relative permeability calculations from two-phase flow simulations directly on digital images of porous rocks. Transp. Porous Media. https://doi.org/10.1007/s11242-011-9877-8 (2012)
Ramstad, T., Øren, P.E., Bakke, S.: Simulation of two-phase flow in reservoir rocks using a lattice Boltzmann method (2010). https://doi.org/10.2118/124617-PA
Reis, T., Phillips, T.: Lattice Boltzmann model for simulating immiscible two-phase flows. J. Phys. A: Math. Theor. **40**(14), 4033 (2007)
Roberts, J.N., Schwartz, L.M.: Grain consolidation and electrical conductivity in porous media. Phys. Rev. B **31**(9), 5990 (1985)
Rothman, D.H., Zaleski, S.: Lattice-Gas Cellular Automata: Simple Models of Complex Hydrodynamics, vol. 5. Cambridge University Press, Cambridge (2004)
Schwartz, L.M., Auzerais, F., Dunsmuir, J., Martys, N., Bentz, D.P., Torquato, S.: Transport and diffusion in three-dimensional composite media. Phys. A: Stat. Mech. Appl. **207**(1–3), 28–36 (1994)
Schwartz, L.M., Martys, N., Bentz, D.P., Garboczi, E.J., Torquato, S.: Cross-property relations and permeability estimation in model porous media. Phys. Rev. E **48**(6), 4584 (1993)
Shan, X.: Analysis and reduction of the spurious current in a class of multiphase lattice Boltzmann models. Phys. Rev. E **73**(4), 047,701 (2006)
Shan, X., Chen, H.: Lattice Boltzmann model for simulating flows with multiple phases and components. Phys. Rev. E **47**(3), 1815 (1993)

Shan, X., Chen, H.: A general multiple-relaxation-time Boltzmann collision model. Int. J. Mod. Phys. C **18**(04), 635–643 (2007)
Shan, X., He, X.: Discretization of the velocity space in the solution of the Boltzmann equation. Phys. Rev. Lett. **80**(1), 65 (1998)
Sheng, Q., Thompson, K.: A unified pore-network algorithm for dynamic two-phase flow. Adv. Water Resour. **95**, 92–108 (2016)
Sheppard, A., Sok, R., Averdunk, H.: Improved pore network extraction methods. In: International Symposium of the Society of Core Analysts, vol. 2125 (2005)
Singh, M., Mohanty, K.: Dynamic modeling of drainage through three-dimensional porous materials. Chem. Eng. Sci. **58**(1), 1–18 (2003). https://doi.org/10.1016/S0009-2509(02)00438-4
Succi, S.: The Lattice Boltzmann Equation: For Fluid Dynamics and Beyond. Oxford University Press, Oxford (2001)
Succi, S.: Lattice Boltzmann 2038. EPL (Europhysics Letters) **109**(5), 50,001 (2015)
Succi, S., Foti, E., Higuera, F.: Three-dimensional flows in complex geometries with the lattice boltzmann method. EPL (Europhysics Letters) **10**(5), 433 (1989)
Sukop, M.C., Thorne, D.T.: Lattice Boltzmann Modeling, an Introduction for Geoscientists and Engineers. Springer, Berlin (2006)
Sussman, M., Puckett, E.G.: A coupled level set and volume-of-fluid method for computing 3D and axisymmetric incompressible two-phase flows. J. Comput. Phys. **162**(2), 301–337 (2000)
Sweijen, T., Hassanizadeh, S.M., Chareyre, B., Zhuang, L.: Dynamic pore-scale model of drainage in granular porous media: the pore-unit assembly method. Water Resour. Res. https://doi.org/10.1029/2017WR021769
Swift, M.R., Osborn, W., Yeomans, J.: Lattice Boltzmann simulation of nonideal fluids. Phys. Rev. Lett. **75**(5), 830 (1995)
Thompson, K.: Pore-scale modeling of fluid transport in disordered fibrous materials. AIChE J. **48**(7), 1369–1389 (2002). https://doi.org/10.1002/aic.690480703
Thompson, K.E., Willson, C.S., Zhang, W.: Quantitative computer reconstruction of particulate materials from microtomography images. Powder Technol. **163**, 169–182 (2006)
Thovert, J., Salles, J., Adler, P.: Computerized characterization of the geometry of real porous media: their discretization, analysis and interpretation. J. Microsc. **170**(1), 65–79 (1993)
Tölke, J.: Implementation of a lattice Boltzmann kernel using the compute unified device architecture developed by nVIDIA. Comput. Vis. Sci. **13**(1), 29 (2010)
Tölke, J., Freudiger, S., Krafczyk, M.: An adaptive scheme using hierarchical grids for lattice Boltzmann multi-phase flow simulations. Comput. Fluids **35**(8–9), 820–830 (2006)
Wildenschild, D., Sheppard, A.P.: X-ray imaging and analysis techniques for quantifying pore-scale structure and processes in subsurface porous medium systems. Adv. Water Resour. **51**, 217–246 (2013). https://doi.org/10.1016/j.advwatres.2012.07.018
Wilkinson, D., Willemsen, J.F.: Invasion percolation: a new form of percolation theory. J. Phys. A: Math. Gen. **16**(14), 3365 (1983)
Xiong, Q., Baychev, T.G., Jivkov, A.P.: Review of pore network modelling of porous media: experimental characterisations, network constructions and applications to reactive transport. J. Contam. Hydrol. **192**, 101–117 (2016)
Yang, J., Boek, E.S.: A comparison study of multi-component lattice Boltzmann models for flow in porous media applications. Comput. Math. Appl. **65**(6), 882–890 (2013)
Yin, X., Zhang, J.: An improved bounce-back scheme for complex boundary conditions in lattice Boltzmann method. J. Comput. Phys. **231**(11), 4295–4303 (2012). https://doi.org/10.1016/j.jcp.2012.02.014
Youssef, S., Rosenberg, E., Deschamps, H., Oughanem, R., Maire, E., Mokso, R.: Oil ganglia dynamics in natural porous media during surfactant flooding captured by ultra-fast X-ray microtomography. In: Proceedings of the Symposium of the Society of Core Analysts, Montpellier, France, pp. 11–18 (2014)
Yuan, H.H., Swanson, B.F.: Resolving pore-space characteristics by rate-controlled porosimetry. SPE Form. Eval. **4**(01), 17–24 (1989)
Yuan, P., Schaefer, L.: Equations of state in a lattice Boltzmann model. Phys. Fluids **18**(4), 042,101 (2006)
Zhu, J., Ma, J.: An improved gray lattice Boltzmann model for simulating fluid flow in multi-scale porous media. Adv. Water Resour. **56**, 61–76 (2013)
Zou, Q., He, X.: On pressure and velocity boundary conditions for the lattice Boltzmann BGK model. Phys. Fluids **9**(6), 1591–1598 (1997)